

Coupled boundary element - characteristics method for elastoplastic problem in rock engineering

YUZO OBARA, AKIRA SATO and KATSUHIKO SUGAWARA

Department of Civil Engineering and Architecture

ABSTRACT

A two-dimensional hybrid numerical method for solving elastoplastic problems in rock engineering is presented by coupling two existing methods, namely, the boundary element method and the characteristics method. This method is called as the coupled Boundary Element - Characteristics Method (BEM-CM). The formulation of this method is presented in order to determine the boundary between elastic and plastic regions and calculate the displacement and strain in the plastic region. It is shown that this method is one of accurate and effective methods for estimating not only the shape and extent of the plastic region but also the state of the displacement and strain in the plastic region around underground opening. Then, some typical examples are solved in order to check the accuracy of the results by this method. Finally, the effectiveness of the BEM-CM to the elastoplastic problem in rock engineering are presented and discussed.

INTRODUCTION

In order to assess the stability of underground openings, it is necessary to clarify the state of stress and deformation of the surrounding rock mass. Because that the shape and extent of plastic region, the states of stress, displacement and strain around the underground openings induced by the excavation are govern the stability of the underground openings. For this purpose, various numerical techniques for elastoplastic problem have been proposed. The finite element method has been widely used up to date among others.^{1,2} A coupled finite element-boundary element method is also attractive.^{3,4} However, when the finite element method is used, a numerical model has to be divided into numerous small elements to obtain a highly accurate solution for the elastoplastic analysis. Furthermore, a semi-analytical model which is a combination of the analytical solution with the characteristics method was proposed to investigate the two-dimensional elastoplastic behavior around a cylindrical opening.⁵ However, since the analytical solution for the elliptic cavity is used to obtain the stress field in the elastic region, it is difficult to apply this method to an opening of arbitrary shape and multiple openings.

This paper presents a new method for the elastoplastic analysis of the underground openings in homogeneous and isotropic media.⁶⁻¹³ It is a two-dimensional coupled boundary element-characteristics method (BEM-CM) to solve the passive earth pressure problem. The characteristics method (CM) is an accurate method to solve plastic equilibrium problems expressed as hyperbolic-type partial differential equations.¹⁴⁻¹⁶ On the other hand, the boundary element method (BEM) is effective for solving boundary value problems of infinite homogeneous elastic domains.¹⁷⁻¹⁹

The coupled BEM-CM method makes full use of the advantages of the BEM and the CM and

the analytical region is divided into two regions, namely elastic region and plastic region. The former is analyzed by the BEM, and the latter is analyzed by the CM. Each region is independently analyzed and the boundary between the elastic region and the plastic region is incrementally modified and expanded from the free surface until the stress state at the boundary between the two regions satisfies a chosen yield function. Thus, this method enables the analysis of the elastoplastic problem for an arbitrary opening shape and multiple openings because of adoption of the BEM for the elastic region. Furthermore, the displacement and strain field in the plastic region around the underground openings can be obtained in detail. However, since the associated flow rule is adopted to compute the displacement and strain in the plastic region by the CM, there has been a tendency that the displacement and strain are estimated more than actual values.

In this paper, the formulation of the BEM-CM is described as well as the limitation of its applicability. The application of this method to elastoplastic problems of the underground circular opening under biaxial initial stress field is presented, and the non-associated flow rule is introduced into the BEM-CM to calculate the displacement and strain field in the plastic region around underground openings. It is shown that this method is one of accurate and effective methods for estimating not only the shape and extent of the plastic region but also the states of the displacement and strain in the plastic region around the underground opening. Furthermore, this method is applied to the problems of rectangular opening, horse-shoe shaped opening and rock slope. Then the shape and extent of the plastic region near the free surface and the characteristics of the displacement and strain field in the plastic region are discussed.

FORMULATION OF BEM-CM

Coupling of BEM-CM

The BEM-CM is effective when the yielding of rock mass around underground openings is of compression kind. However, the rock mass around the underground openings not only yields because of compressive stresses but also fractures due to tensile stresses.

First of all, the limitation of the applicability of this method is discussed with the problem of a circular opening as an example. According to the theory of elasticity, the tangential stress σ_t on the wall of a circular opening under a biaxial initial stress field σ_x^∞ and σ_y^∞ (the compressive stress is defined by positive) is given as follows:

$$\sigma_t = \sigma_x^\infty + \sigma_y^\infty - 2(\sigma_x^\infty - \sigma_y^\infty)\cos 2\theta \quad (1)$$

In regard to σ_t , tensile stresses are generated on the wall of the circular opening under the initial stress field in region I, as shown in Figure 1. In the figure, S_c is the uniaxial compressive strength of rock mass. On the other hand, under the initial stress field in regions II, III and IV, compressive stresses are generated on the whole circumference of the circular opening. In particular, a compressive stress larger than S_c is generated on the whole circumference of the circular opening in region IV and induced partially on the wall of the opening in region III. Consequently, the boundary value problem under the initial stress field in regions III and IV, of which the ratio of horizontal initial stress to vertical initial stress, m is more than $1/3$, can be solved by the BEM-CM.

Now, let us consider an underground opening as illustrated in Figure 2 and suppose that the ground surrounding the opening consists of elastic region Ω_1 and the plastic region Ω_2 . The

elastic region is assumed to behave as an isotropic and homogeneous linear elastic material and the plastic region as an isotropic plastic material which is characterized by a yield function. Figure 2(a) shows the full yielding of the circumference of the opening while Figure 2(b) shows the partial yielding of the circumference of the opening, in which the surface consists of the elastic segment Γ_1 and the plastic segment Γ_2 . In both cases, the boundary between Ω_1 and Ω_2 is defined by Γ_3 , which is so-called elastoplastic interface.

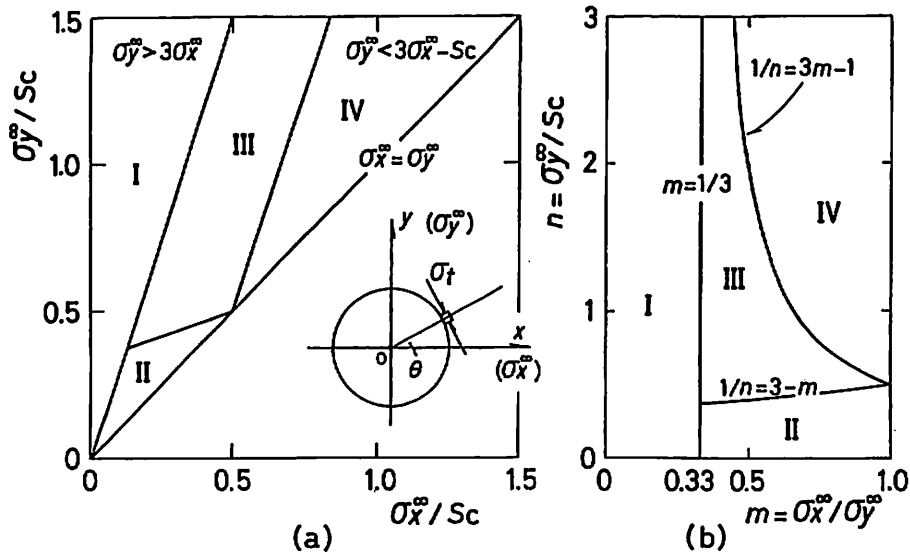


Figure 1 Classification of initial stress for the stress state on the circumference of a circular opening.

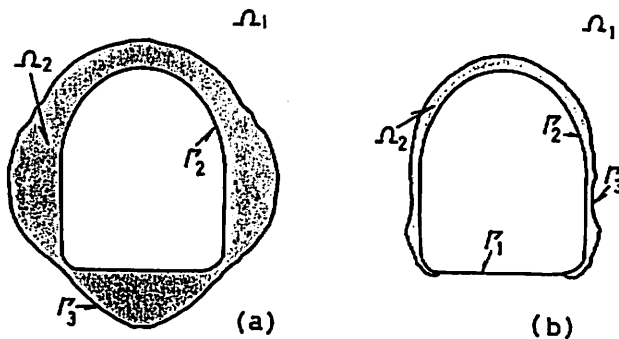


Figure 2 Plastic region Ω_2 around an opening: (a) full yielding of the circumference; (b) partial yielding of the circumference.

If the yield function of the ground is specified by $f(\sigma_{ij})=0$, defining σ_{ij}^o as the stress tensor in Ω_1 and σ_{ij}^p as the stress tensor in Ω_2 , the stress state within Ω_1 is under the condition of $f(\sigma_{ij}^o) \leq 0$ and that in Ω_2 is under the condition of $f(\sigma_{ij}^p) = 0$. Considerations of equilibrium demand that the stress components normal and parallel to Γ_3 should be the same on both side of Γ_3 , as well as the displacement components.

The main problem is how to determine the geometrical shape of the plastic region. For this purpose, the CM is jointly used with the BEM, and the geometrical shape of the plastic region is determined with an iterative procedure, which is the step-by-step widening of the plastic region from the free surface. The CM is used to solve the equilibrium equation within the plastic region and to determine the slip-line field as shown in Figure 3, which indicates an example of the slip-line field around a complete opening in the case that the ground surrounding the opening consists of a plastic material. On the other hand, the BEM is used to obtain the stress field in the elastic region.

Firstly, Γ_2 is evaluated with the condition of $f(\sigma_{ij}^o) \geq 0$, after the elastic stress distribution on the wall of the opening is calculated by the BEM. Secondly, the slip-line field in the area ABC around the opening is analyzed by the CM, assuming that Γ_2 is the base of the plastic region as illustrated in Figure 3. Then the stress σ_{ij}^p within the area ABC is determined. Subsequently, a curve Γ_3 at a described distance from Γ_2 in the area ABC is assigned as an approximation of the elastoplastic interface. The distance is defined as the shortest distance from the opening wall to the points where the slip lines calculated from adjacent discretized points on Γ_2 intersect each other. Therefore, this distance depends on the length of the boundary elements. Then, the stress σ_{ij}^o in the elastic region is analyzed by the BEM, applying the principle of the superposition as illustrated in Figure 4.

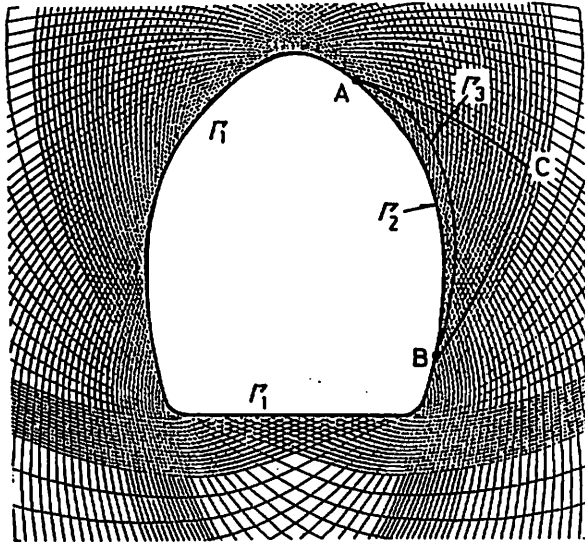


Figure 3 Passive slip line field around an opening and curvilinear triangle ABC on Base Γ_2 .

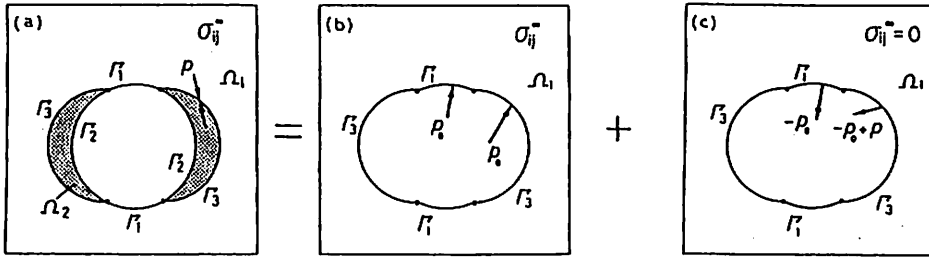


Figure 4 Principle of the superposition: (a) partial yielding of a circular opening; (b) initial stress field; (c) stress change in elastic region.

In Figure 4, the state (a) shows a partial yielding of the circular opening, being subjected to the initial stress field σ_{ij}^∞ at infinity. The traction on the elastoplastic interface Γ_3 is represented by p . The state (b) shows the initial state of the elastic region, being subjected to the initial stress at infinity. The traction p_0 on Γ_1 and Γ_3 is equivalent to σ_{ij}^∞ . The state (c) shows the stress change induced by the excavation and the appearance of the plastic region without the initial stress, namely, the traction $-p_0$ on Γ_1 and the traction $-p_0 + p$ on Γ_3 . The stress field within the elastic region of the state (a) is obtained by superposing the state (c) on the state (b). Since the traction p can be calculated from the stress σ_{ij}^p by Cauchy's formula in the elastic analysis, the continuity of the stress across Γ_3 is always satisfied everywhere.

By examining the stress σ_{ij}^p on Γ_1 and Γ_3 , if there is a range of $f(\sigma_{ij}^p) \geq 0$ on Γ_1 , it is added to Γ_2 , and if there is a range of $f(\sigma_{ij}^p) \geq 0$ on Γ_3 , it is translated outwardly and subsequently the plastic region slightly expands. The step-by-step widening of the plastic region and the repetition of the stress analysis for the elastic region is continued until the stress field satisfies the condition $f(\sigma_{ij}^p) \leq 0$ everywhere in the elastic region. This is the fundamental concept of the procedure to determine the geometrical shape of the plastic region.

Additionally, the effect of tunnel support system may be introduced into the BEM-CM as an internal pressure acting on the wall of underground openings. In this case, the slip-line field around the opening is calculated by assuming that the tractions on Γ_1 , Γ_2 and Γ_3 are p_s , $-p_0 + p$ and $-p_0 + p + p_s$, respectively, as shown in Figure 4(c).

The analysis of the displacement and strain field are subsequently performed. The CM is also available for this analysis. At that time, the boundary condition of the displacement is given on the elastoplastic interface. This is the displacement on Γ_3 calculated by the BEM.

In addition, it can be noted that the hardening and softening effect of a material can be easily incorporated in the BEM-CM, since the yield functions used in the plastic region and on the elastoplastic interface can be independently introduced.

Stress field in plastic region

The stress field in the plastic region is obtained by the CM.¹⁴⁻¹⁶ Mohr-Coulomb's criterion is adopted as the yield function, which is expressed as

$$\tau = C + \sigma \tan \phi \quad (2)$$

where τ and σ are shear stress and normal stress, respectively, and C and ϕ are cohesion and internal frictional angle, respectively. Equation (2) can be rewritten in terms of principal stresses σ_1 and σ_3 ($\sigma_1 \geq \sigma_3 > 0$, the compressive stress is defined by positive), as follows:

$$\sigma_1 - \sigma_3 = 2C \cos \phi + (\sigma_1 + \sigma_3) \sin \phi \quad (3)$$

or

$$\sigma_1 = S_c + q\sigma_3$$

$$S_c = 2C \tan\left(\frac{\pi}{4} + \frac{\phi}{2}\right), \quad q = \tan^2\left(\frac{\pi}{4} + \frac{\phi}{2}\right) \quad (4)$$

where S_c is the uniaxial compressive strength.

If we designate the inclination of σ_1 from the x -axis by β as shown in Figure 5(b), the stress components σ_x , σ_y and τ_{xy} in the x - y co-ordinates, within the plastic region, may be expressed as

$$\begin{aligned} \sigma_x &= \sigma_m (1 + \sin \phi \cos 2\beta) + C \cos \phi \cos 2\beta \\ \sigma_y &= \sigma_m (1 - \sin \phi \cos 2\beta) - C \cos \phi \cos 2\beta \\ \tau_{xy} &= (\sigma_m \sin \phi + C \cos \phi) \sin 2\beta \end{aligned} \quad (5)$$

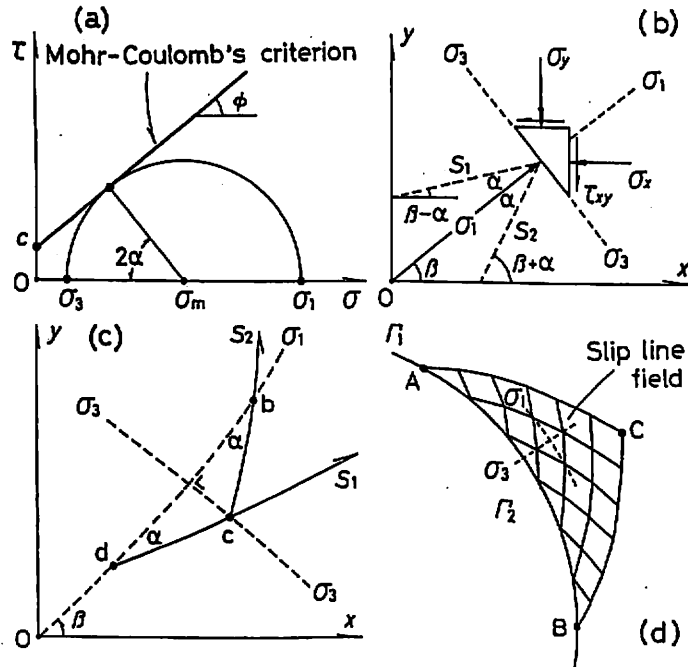


Figure 5 Stress field in plastic region: (a) yield function; (b) x - y co-ordinates and stress components; (c) slip line S_1 and S_2 ; (d) slip line field of the base of Γ_2 .

where $2\sigma_m = \sigma_1 + \sigma_3 = \sigma_x + \sigma_y$, and they have to satisfy the condition of equilibrium as

$$\frac{\partial \sigma_x}{\partial x} + \frac{\partial \tau_{xy}}{\partial y} = 0, \quad \frac{\partial \tau_{xy}}{\partial x} + \frac{\partial \sigma_y}{\partial y} = 0 \quad (6)$$

Substituting Equation (5) into Equation (6), we obtain

$$\begin{aligned} P_1 \frac{\partial \sigma_m}{\partial x} + Q_1 \frac{\partial \sigma_m}{\partial y} + R_1 \frac{\partial \beta}{\partial x} + T_1 \frac{\partial \beta}{\partial y} &= 0 \\ P_2 \frac{\partial \sigma_m}{\partial x} + Q_2 \frac{\partial \sigma_m}{\partial y} + R_2 \frac{\partial \beta}{\partial x} + T_2 \frac{\partial \beta}{\partial y} &= 0 \end{aligned} \quad (7)$$

where

$$\begin{aligned} P_1 &= 1 + \sin \phi \cos 2\beta \\ Q_1 &= P_2 = \sin \phi \sin 2\beta \\ R_1 &= -T_2 = -2(\sigma_m \sin \phi + C \cos \phi) \sin 2\beta \\ T_1 &= R_2 = 2(\sigma_m \sin \phi + C \cos \phi) \cos 2\beta \\ Q_2 &= 1 - \sin \phi \cos 2\beta \end{aligned}$$

Equations (7) are hyperbolic-type partial differential equations for two variables σ_m and β , and the characteristic curves are given by

$$\frac{dy}{dx} = \tan(\beta \pm \alpha), \quad \alpha = \frac{\pi}{4} - \frac{\phi}{2} \quad (8)$$

These characteristic curves coincide with the intersecting slip lines S_1 and S_2 as shown in Figure 5(c).

Since S_1 and S_2 intersect each other at angles $\beta - \alpha$ and $\beta + \alpha$, respectively, the derivatives of the slip lines are expressed as

$$\begin{aligned} \frac{d}{dS_1} &= \cos(\beta - \alpha) \frac{\partial}{\partial x} + \sin(\beta - \alpha) \frac{\partial}{\partial y} \\ \frac{d}{dS_2} &= \cos(\beta + \alpha) \frac{\partial}{\partial x} + \sin(\beta + \alpha) \frac{\partial}{\partial y} \end{aligned} \quad (9)$$

and we obtain the following:

$$\begin{aligned} \cos \phi \frac{\partial}{\partial x} &= \sin(\beta + \alpha) \frac{d}{dS_1} - \sin(\beta - \alpha) \frac{d}{dS_2} \\ \cos \phi \frac{\partial}{\partial y} &= -\cos(\beta + \alpha) \frac{d}{dS_1} + \cos(\beta - \alpha) \frac{d}{dS_2} \end{aligned} \quad (10)$$

Thus, Equation (7) is simplified to

$$\begin{aligned} \frac{d\sigma_m}{dS_1} &= 2(\sigma_m \tan \phi + C) \frac{d\beta}{dS_1} \\ \frac{d\sigma_m}{dS_2} &= -2(\sigma_m \tan \phi + C) \frac{d\beta}{dS_2} \end{aligned} \quad (11)$$

By supposing the segments dc and cb of two intersecting slip lines defined as in Figure 5(c), Equation (11) is replaced by the following linear relations:

$$\begin{aligned}\sigma_{mc} - \sigma_{md} &= 2(\sigma_{md} \tan \phi + C)(\beta_c - \beta_d) \\ \sigma_{mb} - \sigma_{mc} &= -2(\sigma_{mb} \tan \phi + C)(\beta_b - \beta_c)\end{aligned}\quad (12)$$

where the subscripts b, c and d refer to the nodal points in Figure 5(c). The first approximation of σ_{mc} and β_c is obtained by solving Equations (12), because σ_m and β at the nodal points b and d are known. Then, the second approximation of σ_{mc} and β_c is obtained from the fact that the terms $\sigma_{md} \tan \phi$ and $\sigma_{mb} \tan \phi$ in Equations (12) are modified to $0.5(\sigma_{mc} + \sigma_{md}) \tan \phi$ and $0.5(\sigma_{mc} + \sigma_{mb}) \tan \phi$ respectively, using the first approximation of σ_{mc} . The exact solution is obtained after several iterations as described above. On the other hand, the co-ordinates (x_c , y_c) of the nodal point c are obtained by linear difference relations given as

$$\begin{aligned}y_c - y_d &= (x_c - x_d) \tan\left(\frac{\beta_c + \beta_d}{2} - \alpha\right) \text{ on } S_1 \\ y_b - y_c &= (x_b - x_c) \tan\left(\frac{\beta_b + \beta_c}{2} + \alpha\right) \text{ on } S_2\end{aligned}\quad (13)$$

From the theory of the CM, it is known that, if all three stress components are prescribed along the segment AB shown in Figure 5(d) and they satisfy the yield function, the stress state on AB is sufficient to define the stress field uniquely within a curvilinear triangle ABC bounded by the intersecting slip lines through A and B.

Stress field in elastic region

The stress field in the elastic region is obtained by the BEM.¹⁷⁻¹⁹ The boundary integral equation for a two-dimensional boundary value problem can be expressed as follows:

$$\frac{1}{2}u_i(p_0) = \int_{\Gamma} [p_j(p)u_{ji}^*(p, p_0) - p_{ji}^*(p, p_0)u_j(p)] d\Gamma \quad (14)$$

where $u(p_0)$ is the component of displacement at the point p_0 on the boundary Γ , $u_j(p)$ and $p_j(p)$ are the components of the displacement and the traction, respectively, at the point p on Γ and $u_{ji}^*(p, p_0)$ and $p_{ji}^*(p, p_0)$ are the fundamental solutions of the component in the direction j of the displacement and traction at the point p, respectively, when a unit load acts on the point p_0 in the direction i. The boundary integral equation (14) is usually solved numerically by discretizing it into a system of algebraic equations with the aid of a scheme similar to that in the finite element method

$$[H]\{u\} = [L]\{p\} \quad (15)$$

where $[H]$ and $[L]$ are the coefficient matrices and $\{u\}$ and $\{p\}$ are the nodal displacement and traction vectors.

In this paper, the boundary Γ of an underground opening is divided into boundary elements of a given length, as shown in Figure 6(a), to obtain the elastic solution. If these elements are sufficiently small, they will approximate the wall quite closely. In Figure 6(a), P_0^i is a nodal point which is a middle point of the element, and Q_0^i is the connecting point of the boundary elements.

Figure 6(b) shows an example of the model in the case that a plastic region around the opening develops. Due to the step-by-step widening of the plastic region, the connecting point of the element represented by Q_0^i in Figure 6(b) moves away from the wall along the line normal to

the wall, for example, as depicted from Q_0^i to Q^i in Figure 6(b). Since the two pairs of the intersecting slip lines S_1 and S_2 can be drawn through the adjacent points Q^{i+1} and Q^{i-1} , the point Q^i has to be confined within the area bounded by these slip lines as shown in Figure 6(c). This geometrical condition is an indispensable condition for determining the stress field in the plastic region.

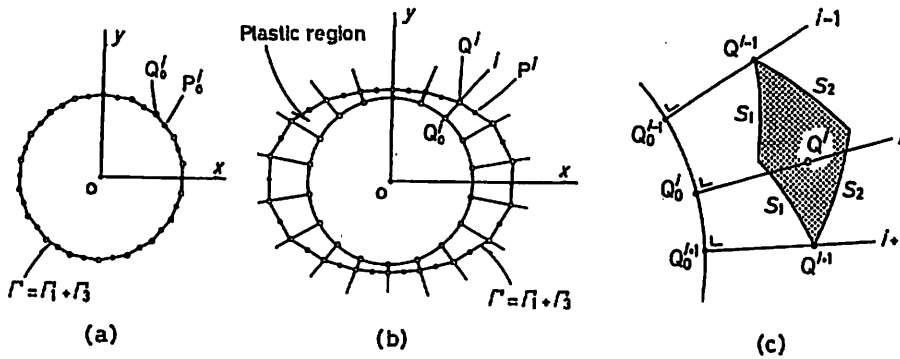


Figure 6 Scheme of boundary element modeling: (a) circular opening model of $\Gamma = \Gamma_1$; (b) boundary model of $\Gamma = \Gamma_3$; (c) geometrical condition for Q^i .

Condition of elastoplastic solution

The stress field in the plastic region has to be uniquely determined by the plastic stress analysis, assuming Γ_2 is the base of the plastic region. Therefore, it is required that the conditions, that Γ_3 exists within the region of ABC as shown in Figure 5(d), and the boundary point Q^i exists within the shaded area, which is bounded by four slip lines drawn through the two adjacent boundary points Q^{i+1} and Q^{i-1} in Figure 6(c), are satisfied.

In addition to the geometrical conditions stated above, the stress state obtained on Γ_3 must satisfy a chosen yield function. To monitor the convergence of the numerical procedure for elastoplastic analysis, we introduce the stress ratio, s to approach the yield function as follows:

$$s = \frac{\sigma_1 - \sigma_3}{\sigma_1^* - \sigma_3^*} \quad (16)$$

where $\sigma_1 - \sigma_3$ is the principal stress difference calculated by the BEM, and $\sigma_1^* - \sigma_3^*$ is the principal stress difference which satisfies the yield function under the condition $\sigma_1 + \sigma_3$. Therefore, the elastoplastic solution is assumed to be achieved, when

$$s = 1.0 \text{ on } \Gamma_3 \text{ and } s < 1.0 \text{ on } \Gamma_1 \quad (17)$$

Displacement in plastic region

The displacement and strain field in the plastic region are also obtained by the CM.¹⁴⁻¹⁶ In this method, Mohr-Coulomb's yield function is adopted to determine the stress field around

underground opening, which is expressed as

$$f = \tau - C - \sigma \tan \phi \quad (18)$$

where τ and σ are the shear and the normal stress respectively, and C and ϕ are the cohesion and the internal friction angle respectively. On the other hand, the plastic potential which is different from the yield function is introduced to calculate displacement field in the plastic region. Accordingly, the non-associated flow rule is used in this method. The plastic potential which is of the same type as the yield function is defined at a plastic stress state as

$$g = \tau - C_p - \sigma \tan \phi_N \quad (19)$$

where C_p is a constant dependent on the plastic stress state and ϕ_N is dilatancy angle. Equations (18) and (19) are rewritten in terms of the principal stresses σ_1 and σ_3 ($\sigma_1 \geq \sigma_3 > 0$, the compressive stress is defined by positive) as

$$f = (\sigma_1 - \sigma_3) - 2C \cos \phi - (\sigma_1 + \sigma_3) \sin \phi \quad (20)$$

$$g = (\sigma_1 - \sigma_3) - 2C_p \cos \phi_N - (\sigma_1 + \sigma_3) \sin \phi_N \quad (21)$$

Now the plastic potential is assumed by using the stress components σ_x , σ_y and τ_{xy} in the x - y co-ordinates as

$$g = \sqrt{(\sigma_x - \sigma_y)^2 + \tau_{xy}^2} - 2C_p \cos \phi_N - (\sigma_x + \sigma_y) \sin \phi_N \quad (22)$$

The non-associated flow rule is defined in terms of the plastic potential expressed as

$$d\{\epsilon^p\} = \lambda' \frac{\partial g}{\partial \{\sigma\}} \quad (23)$$

where λ' is a constant, $\{\ \}$ represents vector and the superscript p refers to the plastic strain. The plastic strain components are defined as

$$\begin{aligned} d\epsilon_x^p &= \lambda' \frac{\partial g}{\partial \sigma_x} = \lambda \left(\frac{\sigma_x - \sigma_y}{2T} - \sin \phi_N \right) \\ d\epsilon_y^p &= \lambda' \frac{\partial g}{\partial \sigma_y} = \lambda \left(\frac{\sigma_y - \sigma_x}{2T} - \sin \phi_N \right) \\ d\gamma_z^p &= \lambda' \frac{\partial g}{\partial \tau_{xy}} = \lambda \left(\frac{\tau_{xy}}{T} \right) \end{aligned} \quad (24)$$

where

$$T^2 = \frac{(\sigma_x - \sigma_y)^2}{4} + \tau_{xy}^2 = \frac{(\sigma_1 - \sigma_3)^2}{4} \quad (25)$$

Designating the inclination of σ_1 from the x -axis by β as shown in Figure 7(a), the stress components in the x - y co-ordinates, within the plastic region, are expressed as

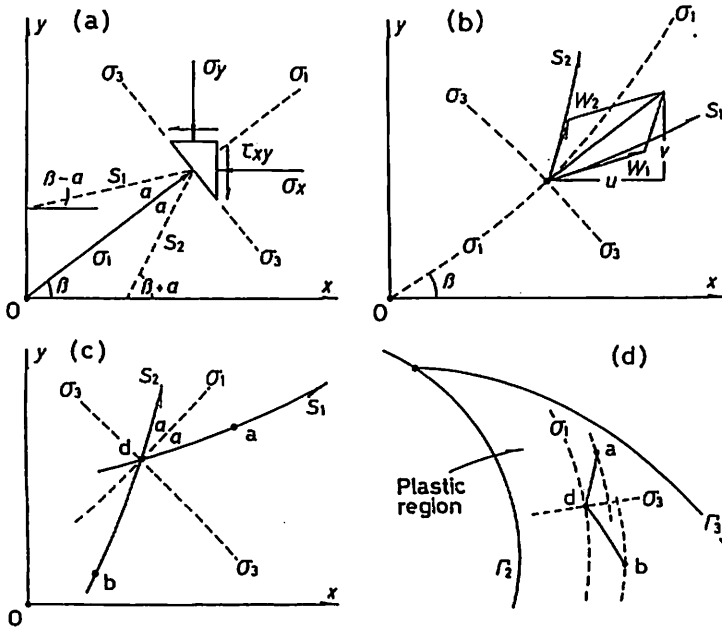


Figure 7 Method of characteristics for displacement analysis in plastic region: (a) co-ordinates and stress component; (b) displacement along slip lines; (c) slip lines S_1 and S_2 , and nodal points; (d) displacement analysis based on the continuity of displacement on Γ_3 .

$$\begin{aligned}\sigma_x &= \frac{\sigma_1 + \sigma_3}{2} + \frac{\sigma_1 - \sigma_3}{2} \cos 2\beta \\ \sigma_y &= \frac{\sigma_1 + \sigma_3}{2} - \frac{\sigma_1 - \sigma_3}{2} \cos 2\beta \\ \tau_{xy} &= \frac{\sigma_1 - \sigma_3}{2} \sin 2\beta\end{aligned}\quad (26)$$

and

$$\sigma_x - \sigma_y = (\sigma_1 - \sigma_3) \cos 2\beta = 2T \cos 2\beta \quad (27)$$

Substituting equation (26) into equation (24), we obtain the following:

$$\begin{aligned}d\epsilon_x^p &= \lambda (\cos 2\beta - \sin \phi_N) \\ d\epsilon_y^p &= -\lambda (\cos 2\beta + \sin \phi_N) \\ d\gamma_{xy}^p &= \lambda \sin 2\beta\end{aligned}\quad (28)$$

Then, the principal plastic strains are given as

$$\begin{aligned}d\epsilon_1^p &= \lambda (1 - \sin \phi_N) \\ d\epsilon_3^p &= -\lambda (1 + \sin \phi_N)\end{aligned}\quad (29)$$

Therefore, the constant λ is obtained by the following equation:

$$\lambda = \frac{d\varepsilon_1^p - d\varepsilon_3^p}{2} \quad (30)$$

By eliminating the constant λ in equation (28), we obtain the following:

$$\begin{aligned} d\varepsilon_x^p - d\varepsilon_y^p &= 2d\gamma_{xy}^p \cot 2\beta \\ d\varepsilon_x^p + d\varepsilon_y^p &= -2d\gamma_{xy}^p \frac{\sin \phi_N}{\sin 2\beta} \end{aligned} \quad (31)$$

Then equation (31) is integrated as follows, by assuming the angle β to be constant at a certain location in the plastic region

$$\begin{aligned} \varepsilon_x^p - \varepsilon_y^p &= 2\gamma_{xy}^p \cot 2\beta \\ \varepsilon_x^p + \varepsilon_y^p &= -2\gamma_{xy}^p \frac{\sin \phi_N}{\sin 2\beta} \end{aligned} \quad (32)$$

On the other hand, the displacement components, u and v are defined in the x - y coordinates in Figure 7(b), expressed as

$$u = u_0 + \Delta u, \quad v = v_0 + \Delta v \quad (33)$$

where u_0 and v_0 are the initial displacement components and Δu and Δv are the displacement due to excavation. Under the initial stress condition, the initial displacement components are given as

$$\begin{aligned} 2Gu_0 &= \{(1-\nu)\sigma_x - \nu\sigma_y\}x + \tau_{xy}y \\ 2Gv_0 &= \{-\nu\sigma_x + (1-\nu)\sigma_y\}y + \tau_{xy}x \end{aligned} \quad (34)$$

where G and ν are the shear modulus and the Poisson's ratio respectively.

The total strain in the plastic region can be obtained as the sum of the elastic strain and the plastic strain, and the strain components are defined by the following equations:

$$\begin{aligned} \varepsilon_x &= \varepsilon_x^e + \varepsilon_x^p = \frac{\partial u}{\partial x} \\ \varepsilon_y &= \varepsilon_y^e + \varepsilon_y^p = \frac{\partial v}{\partial x} \\ \gamma_{xy} &= \gamma_{xy}^e + \gamma_{xy}^p = \frac{1}{2} \left(\frac{\partial u}{\partial y} + \frac{\partial v}{\partial x} \right) \end{aligned} \quad (35)$$

where the superscript e refers to the elastic component. From the elastic stress-strain relation under the plane strain condition, the elastic strain components are given as follows:

$$\begin{aligned} 2G\varepsilon_x^e &= (1-\nu)\sigma_x - \nu\sigma_y \\ 2G\varepsilon_y^e &= -\nu\sigma_x + (1-\nu)\sigma_y \\ 2G\gamma_{xy}^e &= \tau_{xy} \end{aligned} \quad (36)$$

By substituting equations (35) into equations (32), we obtain

$$\begin{aligned} \frac{\partial u}{\partial x} - \cot 2\beta \frac{\partial u}{\partial y} - \cot 2\beta \frac{\partial v}{\partial x} - \frac{\partial v}{\partial y} &= 0 \\ \frac{\partial u}{\partial x} + \frac{\sin \phi_N}{\sin 2\beta} \frac{\partial u}{\partial y} + \frac{\sin \phi_N}{\sin 2\beta} \frac{\partial v}{\partial x} + \frac{\partial v}{\partial y} &= h \end{aligned} \quad (37)$$

where

$$h = \varepsilon_x^e + \varepsilon_y^e + 2\gamma_{xy}^e \frac{\sin \phi_N}{\sin 2\beta} \quad (38)$$

Equations (37) are the hyperbolic-type partial differential equations for u and v , and the characteristics curves coincide with the slip lines S_1 and S_2 in Figure 7(c), as expressed

$$\frac{dy}{dx} = \tan(\beta \pm \alpha), \quad \alpha = \frac{\pi}{4} - \frac{\phi_N}{2} \quad (39)$$

Since S_1 and S_2 intersect each other at angles $\beta - \alpha$ and $\beta + \alpha$ respectively, the derivatives of the slip line are expressed as

$$\begin{aligned} \cos \phi_N \frac{\partial}{\partial x} &= \sin(\beta + \alpha) \frac{d}{dS_1} - \sin(\beta - \alpha) \frac{d}{dS_2} \\ \cos \phi_N \frac{\partial}{\partial y} &= -\cos(\beta + \alpha) \frac{d}{dS_1} + \cos(\beta - \alpha) \frac{d}{dS_2} \end{aligned} \quad (40)$$

and the displacement components in the x - y co-ordinates are represented by the displacement components W_1 and W_2 along the slip lines S_1 and S_2 as shown in Figure 7(b)

$$\begin{aligned} u &= W_1 \cos(\beta - \alpha) + W_2 \cos(\beta + \alpha) \\ v &= W_1 \sin(\beta - \alpha) + W_2 \sin(\beta + \alpha) \end{aligned} \quad (41)$$

By making use of equations (41) and the partial derivatives of equations (40), equations (37) can be rewritten as two differential equations expressing the two variables of W_1 and W_2 along the slip lines.

$$\begin{aligned} \frac{dW_1}{dS_1} + \sin \phi_N \frac{dW_2}{dS_1} - W_2 \cos \phi_N \frac{d\beta}{dS_1} &= \frac{h}{2} \\ \frac{dW_2}{dS_2} + \sin \phi_N \frac{dW_1}{dS_2} + W_1 \cos \phi_N \frac{d\beta}{dS_2} &= \frac{h}{2} \end{aligned} \quad (42)$$

If the segments, ad and db , of two intersecting slip lines are defined as shown in Figure 7(c), equations (42) may be replaced by the linear differential equations for W_1 and W_2 , that is

$$\begin{aligned} W_{1a} - W_{1d} + \sin \phi_N (W_{2a} - W_{2d}) - \cos \phi_N \frac{W_{2a} + W_{2d}}{2} (\beta_a - \beta_d) &= \frac{h_a + h_d}{4} \overline{ad} \\ W_{2d} - W_{2b} + \sin \phi_N (W_{1d} - W_{1b}) + \cos \phi_N \frac{W_{1d} + W_{1b}}{2} (\beta_d - \beta_b) &= \frac{h_d + h_b}{4} \overline{bd} \end{aligned} \quad (43)$$

where \overline{ad} and \overline{db} imply the distance between the nodal points. W_{1a} means the displacement W_1 at the nodal point a . The first approximation of W_{1d} and W_{2d} is obtained by solving equations (43) and may be corrected by step-by-step method.

NUMERICAL EXAMPLES

A circular opening

To demonstrate the accuracy of the solution of BEM-CM, the method is applied to a circular underground opening of radius R under a biaxial initial stress field. The geometrical shapes of the plastic region around the opening due to excavation are shown in Figure 8. The Mohr-Coulomb's criterion is adopted as the yield function and initial stress field, σ_x^∞ and σ_y^∞ , are varied in the analysis together with the plane strain condition. Figure 8(a) shows the result of the shape and radius of the plastic region around the opening under the hydrostatic initial stress field, $m = \sigma_x^\infty / \sigma_y^\infty = 1.0$ and $n = \sigma_y^\infty / S_c = 2.5$, where S_c is the uniaxial compressive strength. The shape and radius of the plastic region around the opening coincide with those by the analytical solution²⁰ given by

$$\frac{R'}{R} = \left[\frac{2\{(q-1)n+1\}}{q+1} \right]^{1/(q-1)} \quad (44)$$

where R' is the radius of the elastoplastic interface. Furthermore, it is confirmed that the stress distribution around the opening agrees with the theoretical one as shown in Figure 9. Figures 8(b) and 8(c) show the shapes of the plastic regions under the initial stress fields, $m = 0.5$, $n = 1.4$ and $m = 0.5$, $n = 2.5$, in regions III and IV, as shown in Figure 1. The stress states calculated on the boundary $\Gamma = \Gamma_1 + \Gamma_3$ are plotted in the space of principal stresses, as

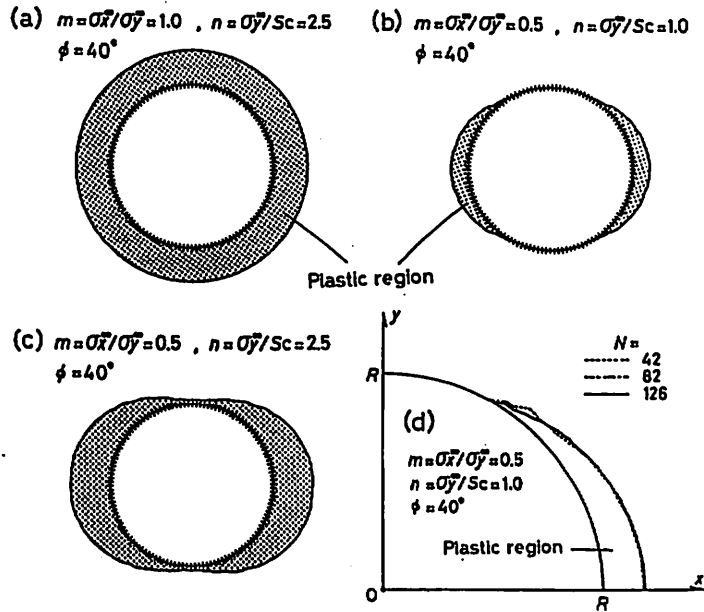


Figure 8 Plastic region around a circular opening under a biaxial stress field: (a) ring shaped plastic region under hydrostatic initial stress field; (b) partial yielding; (c) full yielding; (d) influence of the number of boundary elements, N .

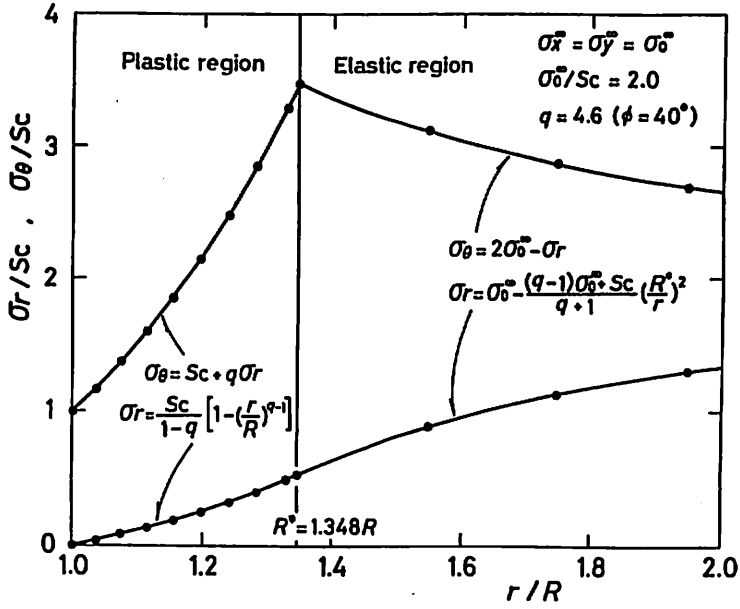


Figure 9 Stress distribution around a circular opening of radius R under hydrostatic initial stress field σ_0^∞ , numerical results (filled circles) and analytical solution (solid line), where r, θ : polar co-ordinates, σ_r, σ_θ : normal stresses.

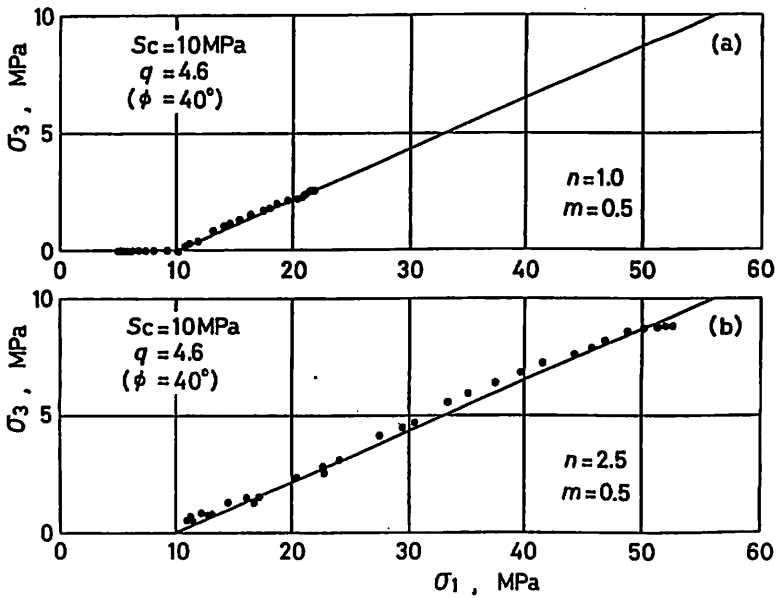


Figure 10 Comparison of analyzed stress on elastoplastic interface with Mohr-Coulomb's criterion.

shown in Figure 10. The stress states on Γ in both cases satisfy the yield function used in this analysis at every point on the elastoplastic interface. Therefore, it is clarified that the elastoplastic solution can be obtained by the BEM-CM with a high accuracy.

The influence of the number of boundary elements, N is shown in Figure 8(d). In the case of $N = 42$, the shape of the plastic region is not smooth in the vicinity where the elastoplastic interface intersects the wall of the opening. The shape of the plastic region becomes smooth as N increases. This means that the finer subdivision of the boundary elements results in more accurate solutions. In addition, the number of iteration to obtain the elastoplastic solution in Figures 8(a), 8(b) and 8(c) are 16, 7 and 19, respectively.

The BEM-CM is applied to the circular opening of the radius R under a hydrostatic initial stress condition, namely $m = \sigma_x^\infty / \sigma_y^\infty = \sigma_0^\infty$ and $n = \sigma_y^\infty / S_c = \sigma_0^\infty / S_c$, to confirm the accuracy of the deformation around the opening. The shear modulus, G and the Poisson's ratio, ν of rock mass are 1.7GPa and 0.2 respectively. In the analysis, the dilatancy angle is changed.

The total displacement, u_r in the radial direction is written as follows¹³:

$$2G \frac{u_r}{r} = \frac{S_c}{1-q} \left\{ (1-\nu) - \frac{(1-\nu)(qq_N+1) - \nu(q+q_N)}{q+q_N} \right\} \left(\frac{r}{R} \right)^{q-1} + \frac{2(1-\nu)}{q+q_N} \{ (q-1)\sigma_0^\infty + S_c \} \left(\frac{R}{r} \right)^{q+1} \quad (45)$$

where $S_c = 2C \tan\left(\frac{\pi}{4} + \frac{\phi}{2}\right)$, $q = \tan^2\left(\frac{\pi}{4} + \frac{\phi}{2}\right)$ and $q_N = \tan^2\left(\frac{\pi}{4} + \frac{\phi_N}{2}\right)$.

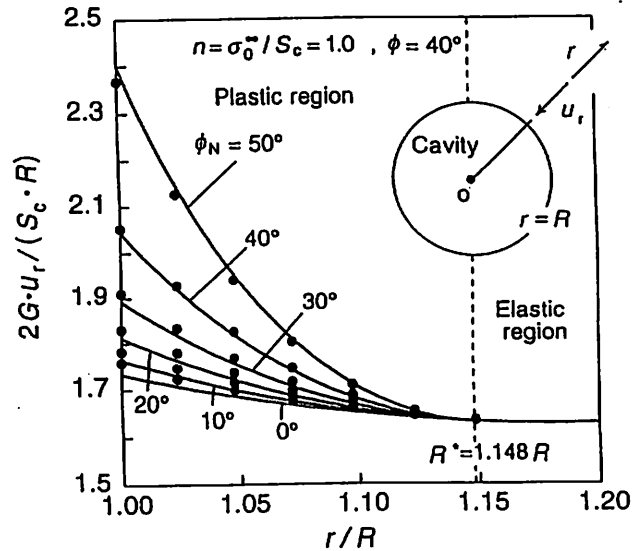


Figure 11 Comparison of numerical results with the theoretical solutions concerning the location of elastoplastic interface and the distribution around a circular opening in the case of using the non-associated flow rule.

Figure 11 shows the comparison of the numerical results with the theoretical solutions. In this figure, the lateral axis is the distance from the opening wall and the longitudinal axis is the normalized displacement, u_r . The black circles are numerical results and the solid lines are the theoretical solutions. The radius of the elastoplastic interface is $1.148R$ and coincides with the theoretical value calculated by equation (44). The numerical distribution of the displacement in the plastic region shows a good agreement with the analytical one in the case of adopting the associated flow rule. On the other hand, the difference between the both results becomes greater with increasing the difference between the internal friction angle ϕ and the dilatancy angle ϕ_N . Because that the integration pass of calculating displacement is not the same as that of calculating stress in the plastic region in the case of adopting the non-associated flow rule. However the maximum error of the displacement on the opening wall is about 1% in the case of $\phi_N = 0^\circ$. Therefore the proposed method is well performed for evaluating the deformation around opening. It is noted that the degree of the deformation decreases with the reduction of ϕ_N .

It is concluded that from this comparison the BEM-CM is an accurate and effective method for estimating not only the shape and extent of the plastic region but also the states of the displacement and strain in the plastic region around underground opening.

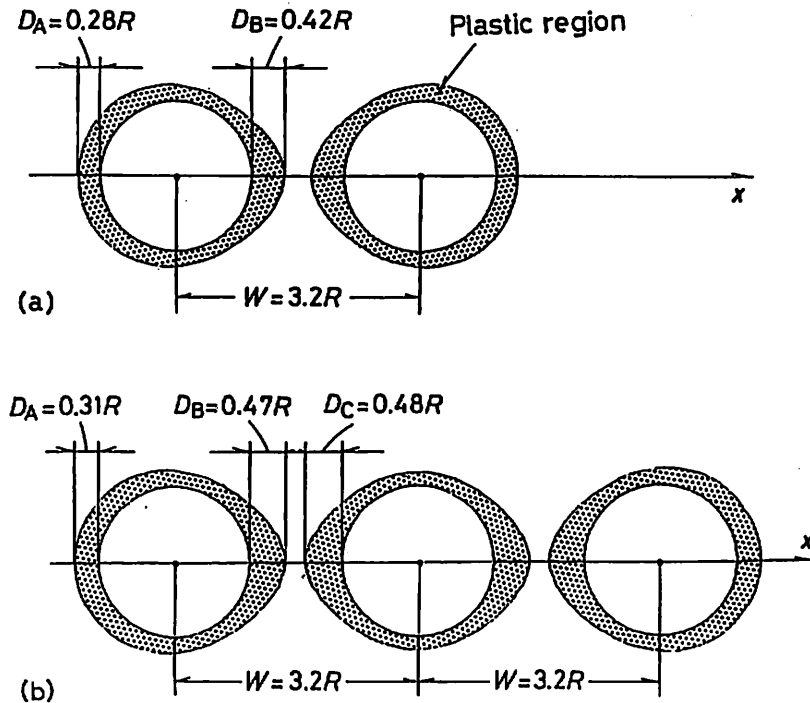


Figure 12 Plastic regions around parallel circular openings in the case of $m = \sigma_x^\infty / \sigma_y^\infty = 1.0$ and $n = \sigma_y^\infty / S_c = 1.5$ and $\phi = 40^\circ$: (a) two parallel openings; (b) three parallel openings.

Multiple Parallel circular openings

The BEM-CM is also effective for obtaining plastic regions around parallel openings. Figures 12(a) and 12(b) shows plastic regions around two and three parallel openings of radius R . The initial stress field is $m = \sigma_x^\infty / \sigma_y^\infty = 1.0$ and $n = \sigma_y^\infty / S_c = 1.5$. The depth of the plastic region around a single circular opening under the same analytical condition is $0.26R$. The greater the number of openings, the larger the depth of the plastic region, particularly in the pillars between openings.

Figure 13 shows the depth of the plastic region depending on the distance between two openings W at the points A and B. When two openings approach each other, the plastic region extends remarkably in the pillar and the pillar is completely yielded in the case of $D_B/R = 0.5$. The difference ΔR between $D_B + R$ and R^* given by Equation (44) is plotted in Figure 14 in the case of $D_B/R > 0.5$ and $m = \sigma_x^\infty / \sigma_y^\infty = 1.0$. In the figure, the difference ΔR and W are normalized by R^* . The relation between ΔR and W is independent of $n = \sigma_y^\infty / S_c$ and can be described by a single curve. This means that the extent of the plastic region in a pillar due to the interaction of openings can be estimated from the radius of the elastoplastic interface R^* by Equation (44) under a hydrostatic initial stress field condition.

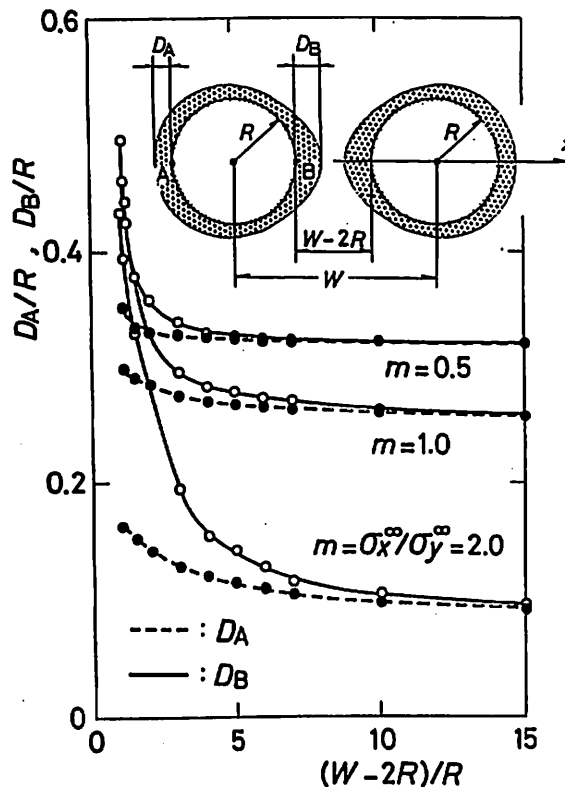


Figure 13 Depth of plastic regions at points A and B depending on the distance between openings ($n = \sigma_y^\infty / S_c = 1.5$ and $\phi = 40^\circ$).

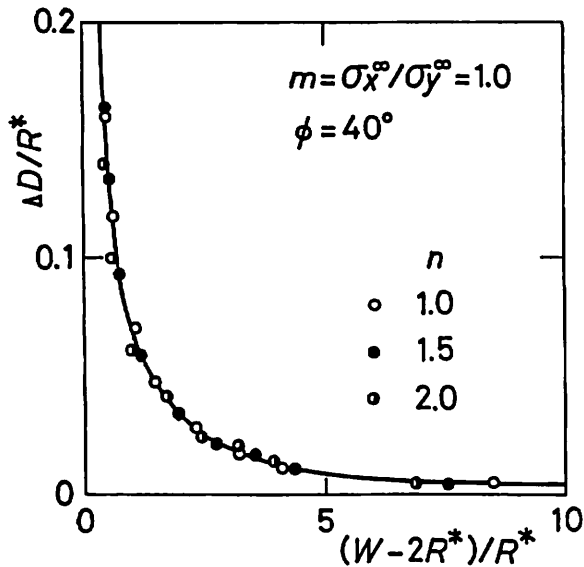


Figure 14 Increase in depth of plastic region in pillar between openings.

Rectangular opening

Figure 15 shows the plastic region around a rectangular opening having corners of the same radius of curvature for a hydrostatic initial stress field. The height and width of the opening are H_y and H_x respectively. The plastic regions first appear at the corners with a small depth and propagate along the surface of the opening as the initial stress $n = \sigma_v^\infty / S_c$ is increased. The depths of the plastic region at roof and sidewalls, defined by D_y and D_x , respectively, are plotted in Figure 16 for a hydrostatic initial stress σ_0 . When the plastic region extends on the whole circumference of the opening with the increase of n , the depth of the plastic region increases rapidly because the rock within the isocles triangle, the base of which is the straight surface and the base angle is as given α , in Equation (8), has to yield under the uniaxial compression parallel to the straight surface. The yielding of a rectangular opening is characterized by this rapid extent of a plastic region.

To examine the characteristics of the displacement and strain in the plastic region around opening, the suggested method is applied to rectangular openings, having a different radius of curvature at corners. The geometry of the openings is shown in Figure 17. The radiuses r_0 of curvature at corner of two openings are $r_0/H_y = 0.026$ in Case 1 and 0.15 in Case 2 respectively. The analytical condition is described in the figure. Figure 18 shows the displacement of the opening surface in the case of adopting the associated flow rule and Figure 19 is that in the case of adopting the non-associated flow rule, $\phi \neq \phi_N = 0^\circ$. The state of elastoplastic displacement of the opening surface is compared with that of elastic displacement in these figures. Δu in the figures represents the displacement. The slip lines are drawn in the plastic region around the openings.

The place which the depth of the plastic region in both cases is largest is located at the center of both side wall. Its depth in Case 2 is 85% of that in Case 1. The depth of the roof and floor in Case 2 is 72% of that in Case 1. It is also found that the depth of the corner in Case 2 is

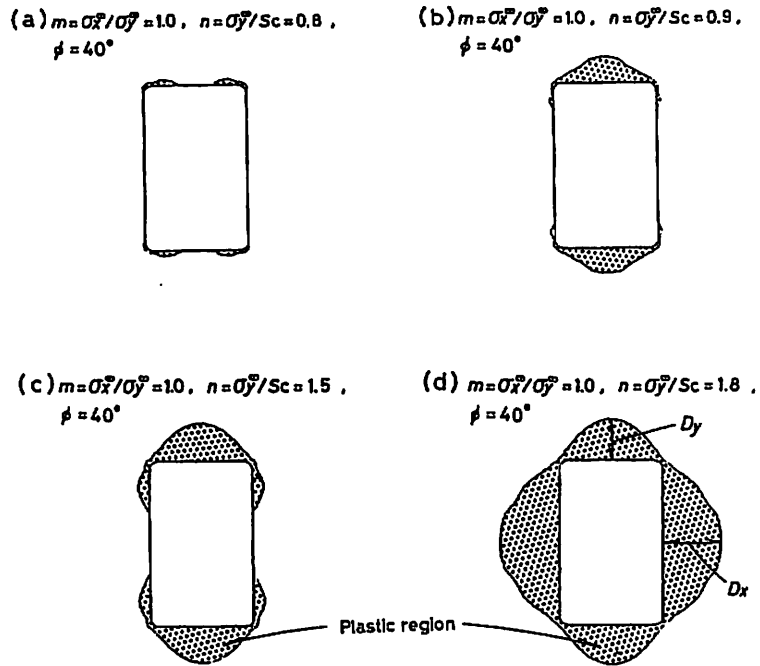


Figure 15 Plastic regions around a rectangular opening in the case of $H_x/H_y = 0.6$, where H_x : width of opening; H_y : height of opening.

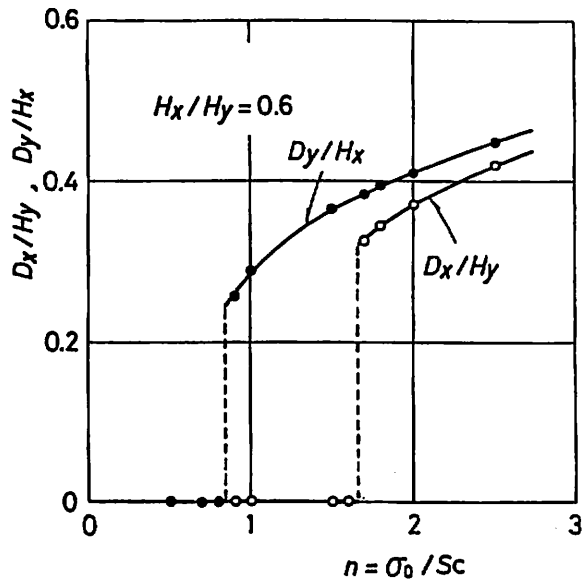
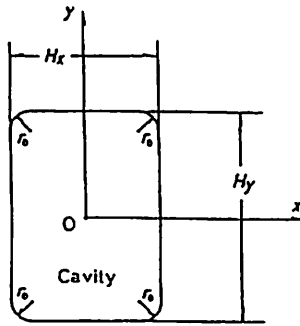


Figure 16 Depth of plastic region D_x and D_y shown in Figure 15(d), depending on $n = \sigma_0 / S_c$.



Analytical condition;

$$\sigma_x^0 = \sigma_y^0 = \sigma_z^0, \quad n = \sigma_0^0 / S_c = 1.8,$$

$$S_c(H_y/2) / 2G = 0.6238, \quad \nu = 0.2, \quad \phi = 40^\circ,$$

$$\text{case 1 : } r_0/H_y = 0.026, \quad \text{case 2 : } r_0/H_y = 0.15$$

Figure 17 A rectangular opening and co-ordinates, and analytical condition.

smaller than that in Case 1. In the case of using the associated flow rule as shown in Figure 18, the elastic displacement of the opening surface maximizes at the center of the side wall. The elastoplastic displacement of it is small at the corner and uniform through the wall. The value of the displacement of the roof and floor in Case 2 is 88% of that in Case 1. It is confirmed that the shape of the rectangular opening having a larger radius of curvature at the corner has a mechanical advantage to decrease the depth of the plastic region and the displacement.

On the other hand, in the case of using the non-associated flow rule as shown in Figure 19, the extent and shape of the plastic region coincide with those in Figure 18. Because that the excavation of the openings is assumed as whole excavation and that the stress and the displacement field around opening are calculated independently in this analysis. Therefore, to simulate actual excavation of the opening, incremental method is necessary to be adopted in the analysis. The elastoplastic displacement decreases, comparing with that in Figure 18. The deformed shape of the surface of the elastoplastic solution is almost the same as that of the elastic solution. It is concluded that the non-dilatant rock mass behaves as the elastic rock mass having the smaller elastic moduli than original ones.

The principal plastic strains is defined by ε_1^p and ε_3^p . The volumetric plastic strain $(\varepsilon_1^p + \varepsilon_3^p)$ is proportional to the maximum plastic shear strain $(\varepsilon_1^p - \varepsilon_3^p)/2$ as follows:

$$\varepsilon_1^p + \varepsilon_3^p = -(\varepsilon_1^p - \varepsilon_3^p) \sin \phi_N \quad (46)$$

Accordingly, the dilatancy is proportional to the differential plastic strain $(\varepsilon_1^p - \varepsilon_3^p)$. In the analysis, the maximum total shear strain $(\varepsilon_1 - \varepsilon_3)/2$ and the maximum elastic shear strain $(\varepsilon_1^e - \varepsilon_3^e)/2$ are calculated at the intersection of slip lines as follows:

$$\begin{aligned} \frac{\varepsilon_1 - \varepsilon_3}{2} &= -\frac{1}{2} \left(\frac{\partial W_1}{\partial S_2} + \frac{\partial W_2}{\partial S_1} \right) \\ \frac{\varepsilon_1^e - \varepsilon_3^e}{2} &= \frac{(1-\nu)(\sigma_1 - \sigma_3)}{2E} \end{aligned} \quad (47)$$

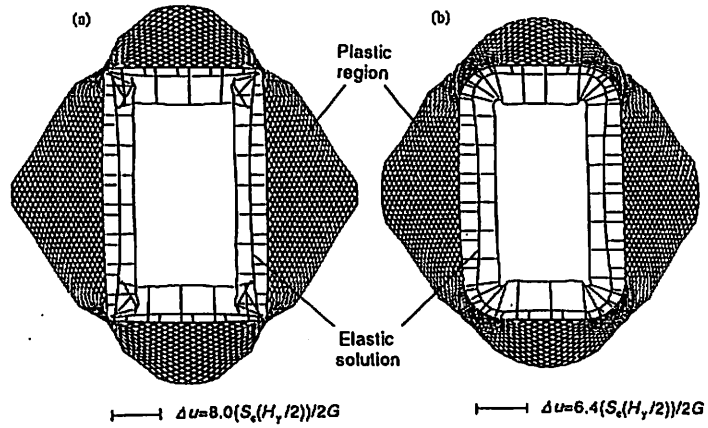


Figure 18 Shape and extent of the plastic region, and displacement of the opening wall in the case of using associated flow rule, dilatancy angle $\phi_N = 40^\circ$ (the slip lines corresponding to the boundary element divided on the elastoplastic interface are drawn in the plastic region): (a) Case 1; (b) Case 2.

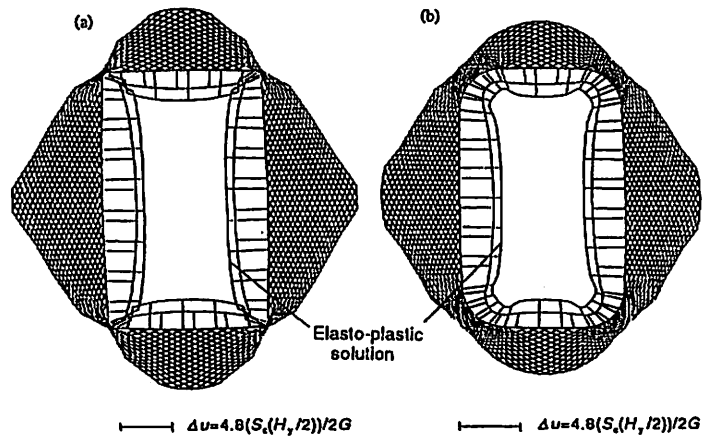


Figure 19 Shape and extent of the plastic region, and displacement of the opening wall in the case of using non-associated flow rule, dilatancy angle $\phi_N = 0^\circ$: (a) Case 1; (b) Case 2.

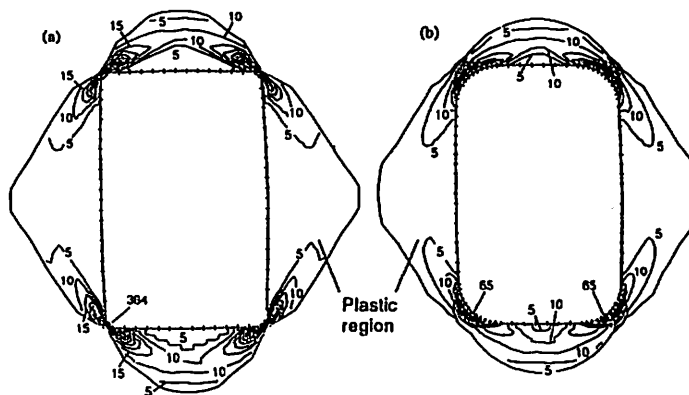


Figure 20 Contour map of the maximum plastic shear strain ($\epsilon_1^p - \epsilon_3^p$) in the plastic region in the case of using associated flow rule, dilatancy angle $\phi_N = 40^\circ$ (unit of numerals in figure is 10^{-3}): (a) Case 1; (b) Case 2.

where E is the Young's modulus. Consequently, the maximum plastic shear strain can be obtained as follows:

$$\frac{\epsilon_1^p - \epsilon_3^p}{2} = \frac{\epsilon_1 - \epsilon_3}{2} - \frac{\epsilon_1^e - \epsilon_3^e}{2} \quad (48)$$

Figure 20 shows the contour map of in the plastic region in the case of $\phi = \phi_N = 40^\circ$. The maximum plastic shear strain is induced at the corner of the opening in both cases. The values of those are 380×10^{-3} in Case 1 and 65×10^{-3} in Case 2 respectively. The value in Case 1 is about six times as large as that in Case 2. The concentration of the contour lines appears near the corner of the opening in both cases. In Case 1, the interval of the contour lines is narrow. The ridge in the contour map coincides with the slip line drawn through the corner of the opening. On the other hand, in Case 2, the interval of the contour lines is more wide, then the value of decreases gradually like a ripple. However the patterns of the contour map in the region less than 5×10^{-3} are almost the same in both cases.

Assuming that the rock mass is fractured through the slip lines when the plastic shear strain reaches its limitation, the fracture surface is considered to be generate along the ridge in the contour map in the plastic region and almost parallel to the elastoplastic interface. It is clear that the shape of the opening in Case 1 can be initiated the fracture surface around the opening greater ease than that in Case 2. If the fracture surface should be generated in both cases, the depth of the intersection of the fracture surface appeared at the center of the sidewall in Case 1 is greater than that in Case 2.

Horse-shoe shaped opening

The displacement and strain field around a house-shaped opening, which is excavated in a rock mass under general biaxial stress state, are shown in Figure 21. The opening is 11.5m in width and 8.5m in height. The radii of the upper part and the both sides of the floor of the opening are

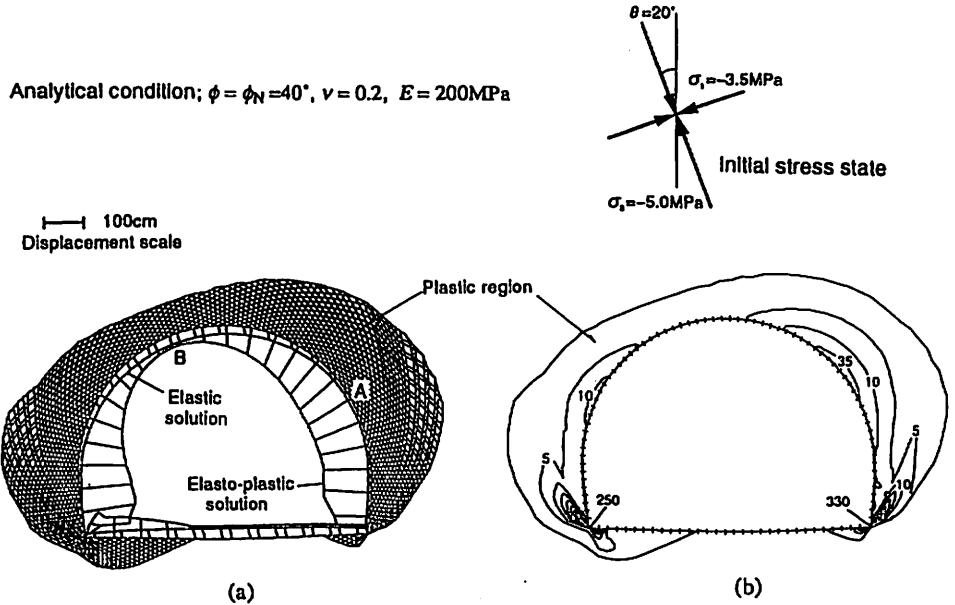


Figure 21 Solution of a horse-shoe shaped opening, which is 11.5m in width and 8.5m in height and the radii of the upper part and the both sides of the floor of it are 5.75m and 0.05m, under biaxial initial state: (a) shape and extent of the plastic region, and displacement of the opening wall; (b) contour map of the maximum plastic shear strain ($\epsilon_1^p - \epsilon_3^p$) in the plastic region (unit of numerals in figure is 10^{-3}).

5.75m and 0.05m.

The slip lines are drawn in the plastic region in Figure 21 (a). The depth of the plastic region near the point A, which is the point in the plane perpendicular to the maximum initial principal stress, is larger than that near the point B, which is in the plane parallel to the maximum initial principal stress, in the arch of the opening. Comparing the elastoplastic displacement with the elastic displacement, the former is larger than the latter. In particular, the difference between them is remarkable near the point A. The latter is large near point A and small near the point B. Conversely the former is small near the point A and large near the point B. Therefore, when the back analysis is performed using the displacements in the plastic region, the direction of the maximum initial principal stress may be made a mistaken estimation as that of the minimum initial principal stress.

The contour map of the plastic shear strain is shown in Figure 21 (b) with the shape of the elastoplastic interface. The concentration of the plastic shear strain appears at the corners of the opening. The ridge of the contour coincides with the slip lines drawn through the corners. This result suggests that the fracture occurs through the corners of the opening and that the fracture surface is not identified with the elastoplastic interface.

From these results, the forming smooth surface of the opening is important from the viewpoint of evading the concentration of the plastic shear strain. It is considered that the shotcrete just after blasting in tunneling might involve the effect of evading the concentration of the shear strain around tunnel. Furthermore, it is desired that the radius of curvature at the corner should be large as much as possible when the opening is constructed.

Rock slope

To investigate the progressive failure mechanism and the premonitory phenomena, the elastoplastic behavior of drained homogeneous rock slope is analyzed using a numerical model in Figure 22. Rock mass is assumed to be a dilatant Mohr-Coulomb's material with self weight, and the associated flow rule is adopted to compute the displacement in the plastic region. Symbols used in the following analysis and the initial condition are shown in Figure 22. Taking the gravitation into account, the vertical and horizontal initial stresses are defined by $\sigma_V = \gamma z$ and $\sigma_H = m\sigma_V$, where z is the depth from the upper ground surface and γ is the unit weight of the rock. In addition, the slope height is noted by the dimensionless parameter: $n = \gamma H/c$. In the BEM analysis, the horizontal displacement is restricted on the boundary FI and HA, and the vertical displacement is fixed to zero on the boundary HI. The segments BC and DE are assumed as a circular arc having a radius, $H/30$ to avoid the singularity.

Figure 23 shows the elastoplastic interfaces in the case of $\theta = 70^\circ$ with $\phi = 30^\circ$, depending on the magnitude of m and n . When the value of m is small, the plastic region propagates upward from the toe of the slope, and the width of the plastic region increases with increasing the value of n . On the other hand, in the case that the value of m is large, the plastic region appears not only along the slope surface but also under the lower horizontal surface, and the depth of the plastic region increases with increasing the value of n . These numerical solutions suggest that the initial stress, particularly the horizontal initial stress, plays an important role in determining the extent of the plastic region.

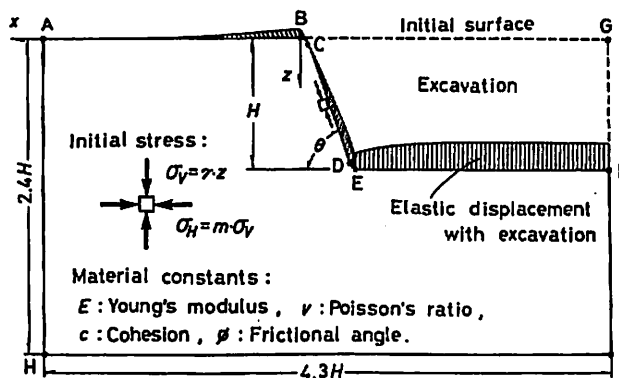


Figure 22 Modelling of rock slope, initial stress condition assumed and material constants.

The displacement distribution within the plastic region can be minutely determined by the present method, as illustrated in Figure 24. In the figure, each arrow indicates the direction and the magnitude of the displacement. The direction of the displacement changes with the distance from the slope surface. Namely, in the deeper region, the vectors are almost vertical in Figure 23(a) and almost parallel to the slope surface in Figure 24(b). Conversely, in the shallow region, the vectors are intersecting with the slope surface having a angle which increases with decreasing the value of m . These results indicate clearly that the expansile displacement near the slope surface is caused by the dilatancy in the plastic region, and that the magnitude of the expansile displacement is in inverse proportion to the internal friction angle, when the associated flow rule is adopted in the analysis.

The plastic strain is directly computed using the displacement profile in Figure 24, as illustrated in Figure 25. The contour of maximum plastic shear strain shows that the concentration of the plastic shear strain appears in all cases at the toe of the slope. The ridge in the contour map coincides with the slip line drawn through the toe of the slope. The numerical results in Figure 25 suggest the occurrence of sliding failure through the toe of the slope. This is compatible with the centrifuge experiments² in Figure 26. Then, it can be concluded that the analysis of the plastic strain by the BEM-CM can provide the minute information to investigate the failure mechanism of the rock slope.

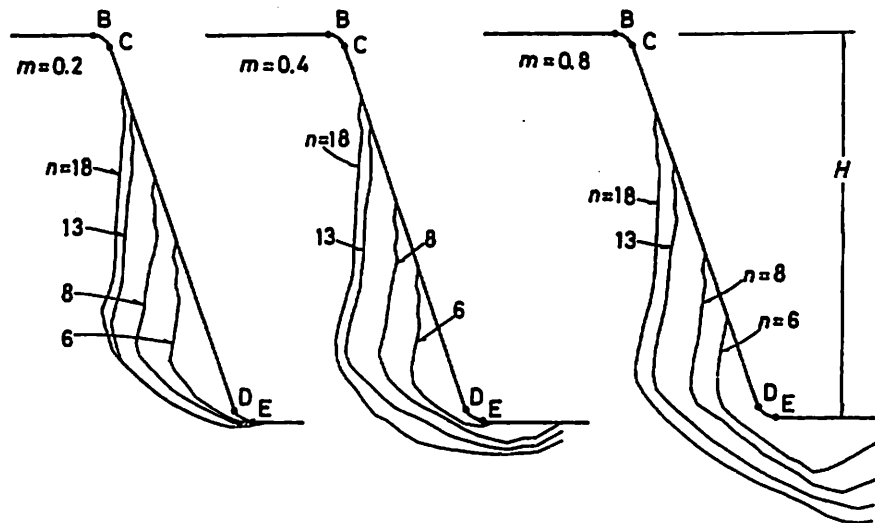


Figure 23 The elastoplastic interface, depending on the parameter $m = \sigma_H / \sigma_V$ and $n = \gamma H / c$, in the case $\theta = 70^\circ$ and $\phi = 30^\circ$

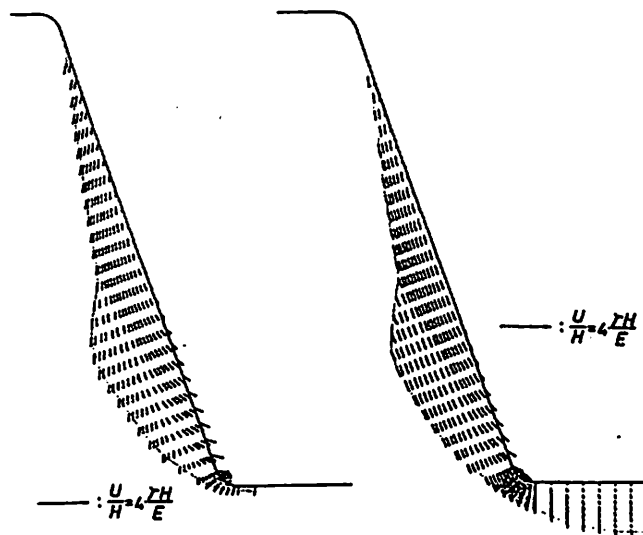


Figure 24 Displacement within plastic region in the case of $\theta = 70^\circ$, $n = 0.2$ and $n = \gamma H/c = 45$: (a) $m = 0.2$; (b) $m = 0.8$.

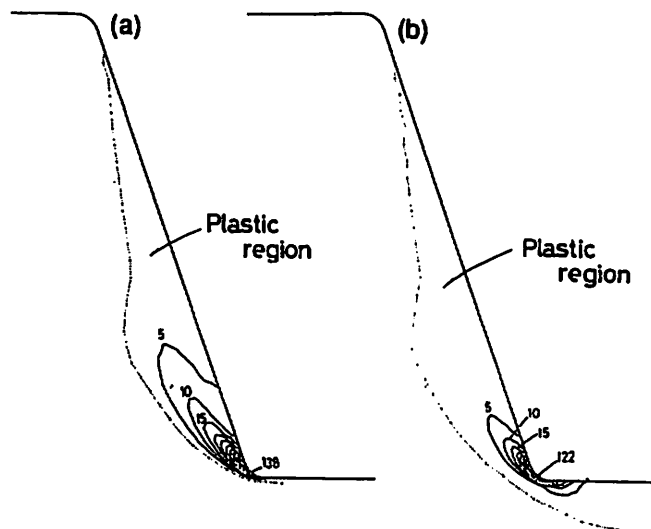


Figure 25 Contour map of the maximum plastic shear strain $E(\epsilon_1^p - \epsilon_3^p) / \gamma H$ in the plastic region, calculated by the displacement in Figure 24: (a) $m = 0.2$; (b) $m = 0.8$.

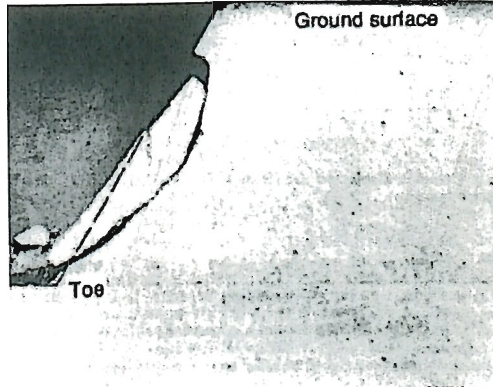


Figure 26 Sliding failure of a wedge shaped area observed by the centrifuge experiment.

CONCLUSION

A new method (BEM-CM), which is a coupling of the boundary element method and characteristics method, is proposed for elastoplastic problem in rock engineering. In this method, the non-associated flow rule is introduced to calculate the displacement and strain field in plastic region.

Firstly, the limitation of applicability of the method concerning the initial stress field was discussed and it was indicated that the stress field around the opening should only allow compressive yielding for which the ratio of horizontal initial stress to vertical initial stress should be greater than $1/3$. Then the formulation of this method was described in order to determine the boundary between elastic and plastic regions and to calculate the displacement and strain in the plastic region. Secondly, this method was applied to elastoplastic problems of a circular underground opening under the biaxial initial stress field. It was concluded that the depth of the plastic region and the state of the stress within the rock mass around the opening were determined with a high accuracy, and that this method was one of accurate and effective methods for solving the excavation problem of underground openings. Thirdly, the plastic region around parallel openings was analyzed by the BEM-CM. It was clarified that the extent of the plastic region in the pillar between openings can be estimated from the analytical solution for a hydrostatic initial stress field. From the results for a rectangular opening, it was shown that the yielding around the rectangular opening is characterized by the rapid propagation of the plastic region at the floor, roof and sidewalls with the increase of initial stress. Then, it was made clear that the failure mechanism may be investigated from the distribution of the maximum plastic shear strain. Furthermore, it was noted that the shotcrete just after blasting in tunneling involve the effect of evading the concentration of the shear strain around tunnel due to the forming smooth surface of it. Finally, it can be concluded that the present method produces the results within acceptable engineering accuracy to specify the slip line which plays an important role in the progressive failure of rock structure from the successful applications to underground openings and rock slope.

In addition, the material behavior considered in the present paper is elastic-perfectly plastic.

Therefore, the stress field in plastic region as well as the interface between elastic region and plastic region obeys the yield function. However, since these yield functions can be independently introduced, it is possible that the hardening or softening effect of a material can be easily incorporated in the BEM-CM.

REFERENCES

1. O. C. Zienkiewicz, *The Finite Element Method*, 3rd ed, McGraw-Hill, New York, 1977.
2. D. R. J. Owen and E. Hinton, *Finite Elements in Plasticity, Theory and Practice*, Pineridge Press, Swansea, 1980.
3. Y. Mitsui, Y. Ichikawa, Y. Obara and T. Kawamoto, 'A coupling scheme for boundary and finite elements using a joint element', *Int. j. numer. anal. methods geomech.*, **9**, 161-172 (1985).
4. G. Beer, 'Implementation of combined boundary element-finite element analysis applications in geomechanics', in *Developments in Boundary Elements-4*, Elsevier Applied Science Publications, Amsterdam, 1986, pp.191-225.
5. E. Detournay and C. Fairhurst, 'Two-dimensional elastoplastic analysis of a long, cylindrical cavity under non hydrostatic loading', *Int. J. Rock Mech. Min. Sci. Geomech. Abstr.*, **24**, (4), 197-211 (1987).
6. K. Sugawara, T. Aoki and Y. Suzuki, 'A coupled BEM-CM for elastoplastic analysis of underground openings', *Proc. of 19th Symp. on Rock Mech.*, Tokyo, 1987 pp.226-270.
7. K. Sugawara, T. Aoki and Y. Suzuki, 'Elasto-plastic analysis of rock caverns by a coupled boundary element-characteristics method', *J. Mining Metall. Int. Japan*, **104**, 261-266 (1988).
8. K. Sugawara, T. Aoki and Y. Suzuki, 'A coupled boundary element-characteristics method for elastoplastic analysis', *Proc. of ISRM Symp. Rock Mechanics and Power Plant*, 1988, pp.249-258.
9. T. Aoki, K. Sugawara, Y. Obara and Y. Suzuki, 'Elasto-plastic deformation of a circular opening under biaxial stress condition', *J. Mining Metall. Int. Japan*, **104** 489-494 (1988).
10. T. Aoki and K. Sugawara, 'Elasto-plastic analysis of a single rectangular opening and parallel circular openings under biaxial stress condition', *J. Mining Metall. Int. Japan*, **105**, 511-516 (1989).
11. Y. Obara, T. Nakayama, H. Okamura and T. Akimoto, 'Coupled boundary element-characteristics method and its application to elastoplastic problem in rock engineering', *Proc. of the Int. Symp. on Assessment and Prevention of Failure Phenomena in Rock Engineering*, Turkey(Istanbul), pp.927-933,1993
12. Y. Obara, T. Aoki, H.K. Jang, T. Nakayama and K. Sugawara, 'Determination of plastic regions around underground openings by a coupled boundary element-characteristics method', *Int. J. Numer. Anal. Methods Geomech.*, **16**, 701-716 (1992).
13. Y. Obara and K. Sugawara, 'Elastoplastic deformation around underground openings under biaxial initial stress field', *Int. J. Numer. Anal. Methods Geomech.*, **21**, 721-737 (1997).
14. R. Hill, *The Mathematical Theory of Plasticity*, Oxford University Press, Oxford, 1950.
15. T. Mogami, *Soil Mechanics*, Gihoudou, pp.746-891 1969.
16. L. M. Kachznov, *Foundations of the Theory of Plasticity*, North-Holland, Amsterdam, 1971.
17. P. K. Banerjee and R. Butterfield, *Boundary Element Methods in Engineering*, MacGraw-Hill, New York, 1981.

18. S. Kobayashi 'Applications of boundary integral equation method to geomechanics', *Proc. of 5th Int. Conf. on Numerical Method in Geomechanics*, Nagoya, Vol.1, 1985, 83-92.
19. C. A. Brebbia, *The Boundary Element Method for Engineers*, Pentech Press, Plymouth, 1978.
20. J. C. Jaeger and N. G. W. Cook, '*Fundamentals of Rock Mechanics*', Chapman and Hall, London 1968.
21. H. Okamura, K. Sugawara, M. Akimoto, S. Kubota & O. Kaneshige, 'Experimental study on rock slope stability by the use of a centrifuge', *J. Mining and Metallurgical Institute of Japan*, 104, 7-4 (1979).